VTT Technical Research Centre of Finland

Micromechanics driven design of ferritic-austenitic duplex stainless steel microstructures for improved cleavage fracture toughness

Laukkanen, Anssi; Uusikallio, Sampo; Lindroos, Matti; Andersson, Tom; Kömi, Jukka; Porter, David

Published in:
Engineering Fracture Mechanics

DOI:
10.1016/j.engfracmech.2021.107878

Published: 01/08/2021

Document Version
Publisher's final version

Engineering Fracture Mechanics 253 (2021) 107878

Contents lists available at ScienceDirect

Engineering Fracture Mechanics

journal homepage: www.elsevier.com/locate/engfracmech

Micromechanics driven design of ferritic–austenitic duplex stainless steel microstructures for improved cleavage fracture toughness

Anssi Laukkanen [a,*], Sampo Uusikallio [b], Matti Lindroos [a], Tom Andersson [a], Jukka Kömi [b], David Porter [b]

[a] Integrated Computational Materials Engineering, VTT Technical Research Centre of Finland Ltd., Espoo, Finland
[b] University of Oulu, Center for Advanced Steel Research, Oulu, Finland

ARTICLE INFO

Keywords:
Lean duplex
Stainless steels
Crystal plasticity
Micromechanics
μWST
Cleavage fracture
Brittle fracture

ABSTRACT

Ferritic–austenitic duplex stainless steels are known to offer favorable combinations of good mechanical properties and corrosion resistance to be used for structural purposes. Lean duplex grades have already been introduced for consideration to replace standard 18–8 austenitic stainless steels in various industrial applications. Ferrite and austenite represent different deformation behaviors and contribute to the resulting fracture toughness characteristics. Micromechanical crystal plasticity based assessment of this cleavage fracture behavior is the subject area of current work. The objective is to bridge cleavage fracture models to full field crystal plasticity imaging based modeling of microstructures of ferritic–austenitic duplex stainless steels. The goal is to introduce means to computationally assess the effects of different multi-phase microstructural morphologies to cleavage fracture toughness and develop both the respective constitutive and cleavage fracture modeling capabilities. Such means can be used as an aid to develop better cleavage resistant, while in the current context lean, steel grades. Three different steels are investigated with differing austenite phase morphologies, and their behavior with respect to fracture mechanical response evaluated by micromechanical modeling. The effect of austenite fraction and morphology in terms of improving fracture toughness, a critical parameter concerning these steel grades and improvement of their cleavage fracture properties, is investigated. Deleterious features such as large ferrite grain size and microstructural property mismatching are identified and their implications to fracture toughness and development of applicable modeling capabilities for ferritic–austenitic duplex steels discussed. Simple design task of varying the austenite phase fraction is performed using synthetic microstructural modeling and the results evaluated with respect to their influence on the fracture toughness ductile-to-brittle transition.

1. Introduction

Ferritic–austenitic duplex stainless steels are known to offer favorable combinations of good mechanical properties and corrosion resistance to be used widely for structural purposes. The ideal ferrite–austenite phase ratio to achieve such qualities has been noted to be 1:1 [1,2]. Lean duplex grades have already been introduced for consideration to replace standard 18–8 austenitic stainless steels in various industrial applications. Lately, research has shown that good transformation-induced plasticity (TRIP) ductility can also be achieved with 30% austenite content [3]. In these steels, keeping the phase ratio unchanged while maintaining sufficient

* Corresponding author.
E-mail address: anssi.laukkanen@vtt.fi (A. Laukkanen).

https://doi.org/10.1016/j.engfracmech.2021.107878
Received 1 December 2020; Received in revised form 26 June 2021; Accepted 5 July 2021
Available online 10 July 2021

Latin

$\dot{v}$	Plastic deformation velocity
x_s	Kinematic hardening parameter
r_s	Isotropic hardening parameter
Q	Isotropic hardening parameter
b	Isotropic hardening parameter
K	Viscosity parameter
n	Viscosity parameter
$\underline{n}^s$	Normal vector
H_{rs}	Interaction matrix
C	Kinematic hardening parameter
D	Kinematic hardening parameter
D^g	Scale transition parameter
$\underline{\underline{L}}$	Modulus
K_0	Normalization fracture toughness
K_{Jc}	Median fracture toughness
P_r	Cleavage initiation probability
P_{fr}	Cleavage failure probability
d_c	Critical initiator size
f	Volume fraction
d	Initiator size
m	Weibull shape parameter
d_N	Initiator size normalization parameter
E_p	Particle elastic modulus
$\bar{d}$	Mean initiator size
P_d	Particle size distribution
$Rp0.2$	Yield stress
Rm	Tensile strength
$A5$	Elongation to fracture
Ag	Uniform elongation
$\underline{\underline{C}}$	Elasticity tensor
h_i	Interaction parameter

Greek

$\dot{\gamma}^s$	Slip system plastic slip rate
τ^s	Resolved shear stress
$\underline{\sigma_g}$	Grain mean stress tensor
τ_0	Shear strength parameter
$\underline{\underline{\beta}}$	Elastoplastic tensor
$\underline{\Sigma}$	Macroscopic average stress tensor
$\underline{\dot{\epsilon}}_p^g$	Rate of local viscoplastic deformation
δ^g	Scale transition parameter
ν	Size distribution shape parameter
σ_p	Particle stress
σ_0	Particle stress normalization parameter
$\underline{\sigma}$	True stress tensor
$\underline{\epsilon}$	Logarithmic strain tensor
σ_{yy}	Matrix stress

stability of austenite has been achieved using Mn and N as partial substitutes to Ni and Mo while adding Cr. Furthermore, alloying N instead of Mo reduces alloying costs without compromising good corrosion resistance. Ferrite and austenite represent different deformation behaviors [4]. High number of possible slip systems leads to deformation driven by dislocation slip to occur in ferrite while deformation of austenite happens mainly due to dislocation slip, twin formation and martensite transformation. Unintentional

ϵ_{yy}	Matrix strain

Acronyms

$TRIP$	Transformation-Induced Plasticity
μWST	Micromechanical WST model
CP	Crystal Plasticity
FE	Finite Element
KAM	Kernel Average Misorientation
RVE	Representative Volume Element
$EBSD$	Electron Backscatter Diffraction
OIM	Orientation Imaging Microscopy
BCC	Body Centered Cubic
FCC	Face Centered Cubic
MC	Master Curve
PDF	Probability Density Function
DBT	Ductile-to-Brittle Transition
$KUBC$	Kinetic Uniform Boundary Condition
LA	Local Approach
$MIBF$	Microstructure Informed Beremin Fracture model
$ICME$	Integrated Computational Materials Engineering

martensite transformation can also happen already during sample preparation especially when preparing lean ferritic–austenitic stainless steels due to high metastability of the austenite phase [5].

Micromechanical modeling involving representation of the microstructural characteristics enables analysis of local stress–strain state and deformation, which can be linked to the strength-to-ductility characteristics of dual phase steels [6,7]. Thus, it can be envisioned that micromechanical modeling at the scale of the ferritic–austenitic steel microstructure can be employed to investigate both the deformation and representative stress states, followingly providing insights as to the sources of strengthening and ductility of the steel as a whole. Micromechanical models for cleavage have typically been formulated based on local cleavage criteria on the basis of statistical modeling of the respective micromechanism, such as in [8–11], a fairly recent review on recent progress and challenges from an engineering perspective presented in [11] by Ruggieri et al. These models are usually in principle applicable for any microstructure where the failure takes place by a weakest link mechanism, but can be argued to lack in microstructural resolution. Recently, an increasing number of approaches have focused on addressing this lack of microstructural full-field by utilizing crystal plasticity (CP) with differing criteria describing the possible onset of failure and its propagation in steels and like materials. Forget et al. [12] suggested a microstructure based brittle failure model for hierarchical microstructures of bainitic steels, including nano-carbides and their added hardening and occasionally embrittling effects to intra-grain and inter-grain deformation characteristics. The work is a part of efforts in introducing a "microstructurally informed" brittle fracture models, and the underlying idea in similar models as in Libert et al. [13] is to capture local deformation behavior of the material in multiscale, whether local phases, defects or special deformation mechanisms such as twinning contribute to strengthening/softening and the failure process. In terms of assessing cleavage failure probability this is the principle adopted also in present work.

With respect to specifically ferrite–austenite containing dual phase steels, the use of CP based micromechanical modeling to better grasp microstructure scale stress–strain response has been still somewhat limited, especially if we consider dual phase microstructures in general and limit ourselves to full field modeling. Kim et al. [14] utilized CP based finite element (FE) modeling to investigate deformation heterogeneity in duplex stainless steel, their work focusing on kinematic phase stability and establishing phase specific deformation response while comparing the model to in-situ neutron diffraction experiments. In [15] Jeong et al. utilized a similar approach as in current work to investigate the deformation response of the multiphase system by directly mapping the microstructure to a FE model. The emphasis was in comparing to experimental findings and investigating how properly their model can capture, for example, kernel average misorientation (KAM) evolution during tensile loading of simplified representative volume elements (RVEs). Bugat et al. [16] used various different complexity level micromechanical models from mean field to bicrystals to assess stress distribution in aged ferritic–austenitic steels, correlating their findings to damage nucleation in the respective microstructures.

In general, these microstructurally informed approaches allow one to couple fine scale features to macroscopic behavior of the materials quite robustly. However, their greatest restriction is that the crack growth from grain to grain and within the material microstructural hierarchies is often not clearly established, for example in fatigue conditions, because lifetime predictions are usually restricted on the nucleation of probable damage sites. Alternative models, such as proposed by Aslan et al. [17], Sabnis et al. [18], and Lindroos et al. [19], aim to capture damage nucleation in the material and provide its evolution during deformation. These usually computationally more costly approaches are able to describe transition from micro-cracks to short crack growth within the microstructure, but inherently lack in robustness due to more complex CP formulations. The objective ultimately is to utilize such

Table 1
Chemical compositions [wt. %].

Steel	Cr	Mn	Mo	Ni	C	N	Si
A	22.0	0.51	0.2	0.1	0.023	0.151	0.3
B	21.9	3.06	0.21	0.1	0.018	0.181	0.32
C	20.3	2.86	0.2	1.1	0.023	0.184	0.31

models also for ferritic–austenitic steels, however, this poses a strain on the parameterization of the models and, for example, the use of advanced characterization techniques, such as small scale in-situ testing is emphasized to produce sufficient data to that effect.

The objective of current work is to bridge cleavage fracture models to full field CP modeling of imaging based microstructural models of ferritic–austenitic duplex stainless steels. The goal is to build capabilities to computationally assess the effects of different microstructural morphologies to cleavage fracture toughness, and as such, a version of the "WST" model (the original model without microstructural links in [8,9]) referred to as the μWST model, which interfaces to CP modeling results of ferritic–austenitic duplex steels. TRIP effects are not included in present paper, but are a subject of a follow up work utilizing the constitutive model presented by the authors in [20] and a future area of research. Three different steel grades are investigated with differing austenite morphologies, and their behavior with respect to fracture mechanical response evaluated by micromechanical modeling. The effects of austenite phase fraction and morphology in terms of improving fracture toughness, critical parameters concerning these steel grades and improvement of their cleavage fracture properties, is investigated.

2. Materials and methods

2.1. Materials

The studied low-Ni ferritic–austenitic stainless steels were laboratory casts. Ingots 48 mm thick were hot rolled using laboratory rolling mill to a 92.7% total reduction for final thickness of 3.5 mm. Annealing at 1100°C for 300 s and water quenching were done instantly after hot rolling. ARL 4460 optical emission spectrometer and an ARL 9800 X-ray spectrometer were used to determine the chemical compositions listed in Table 1.

2.2. Characterization

Preliminary phase fractions were studied using Satmagan and Feritscope (Helmut Fisher FMP30) instruments. Samples for this purpose were prepared using mechanical polishing. Electropolishing according to Uusikallio et al. [5] was conducted for samples prepared for further characterization, namely for electron backscatter diffraction (EBSD).

Microstructural studies were carried on with a field emission scanning electron microscope (FE-SEM, Zeiss Sigma) Combined with an EDAX Hikari XP electron backscatter diffraction (EBSD) camera and an accessory device (EDAX, TSL OIM Data Analysis, OIMDC 7.2.1 [01-23-15]. Acceleration voltage of 15 kV, a working distance of 13.1 mm and a step size of 0.5 um were applied for the measurements. Low magnification of 300x was used in order to obtain sufficient amount of ferrite grains for modeling. The microstructure was studied in both rolling and transverse directions. Phase fractions were also confirmed using EBSD as seen in Table 2. EBSD maps and grain sizes were constructed using Orientation Imaging Microscopy (OIM) 7.1.0 [03-14-14] software.

Phase-specific microhardness measurements were studied using MHT-Z-AE-0000 microhardness tester applying force of 0.1 N. Test results were investigated using Anton Paar Integration 6.2.10 [2015-10-07].

Tensile properties of the studied materials were determined using Zwick Z250/SW5 A tensile testing machine. The tests were carried out according to ISO EN 6892-1 standard together with method A224, which is normally used with austenitic tensile specimens. In the method A224, beginning of the test is executed with strain rate of 1.1 mm/min. As soon as the Rp values of the sample are completed, the strain rate is raised up to 30.2 mm/min. Thus, a jump is observed in stress–strain figures around 1.5% of total elongation.

2.3. Crystal plasticity model

A phenomenological CP was selected to describe dislocation based plasticity in the materials. Rate dependent formulation is used to capture the strain rate sensitivity of the material, as the experiments included strain rate jump tests. Both of the phases, austenite and ferrite, use the same flow rule and hardening equations. The austenite phase involves 12 FCC type of $\{111\}\langle 110\rangle$ slip systems. The plasticity in ferrite phase is represented a total of 24 BCC slip systems, including slip families 12 $\{110\}\langle 111\rangle$ and 12 $\{112\}\langle 111\rangle$. The phases and the respective deformation behaviors are as such treated differently in the following full field microstructural models. The slip rate is presented as:

$$\dot{\gamma}^s = \dot{v}\, sign(\tau^s) = \left\langle \frac{|\tau^s - x^s| - r^s - \tau_0}{K} \right\rangle^n sign(\tau^s - x^s) \tag{1}$$

Table 2
Phase fractions [% Austenite].

Steel	Feritscope	Satmagan	EBSD
A	12.4	14.7	17.7
B	17.3	22.7	25.3
C	44.9	47.1	45.9

where τ^s is the resolved shear stress of a slip system, x^s is the kinematic hardening variable, and r^s is the isotropic hardening variable. Parameters K and n control the viscosity of the material.

$$r^s = Q \sum_r H_{rs}\{1 - exp(-bv^r)\} \tag{2}$$

where Q is the isotropic hardening parameter, b presents saturation of the hardening, and H_{rs} is the interaction matrix for different dislocation interactions, the interaction matrix is presented in the following by its components h_i as also, e.g., in Lindroos et al. [19].

Nonlinear evolution of kinematic hardening was used with two parameters C and D, the respective terms given as:

$$x^s = C\alpha_s \;\; ; \;\; \dot{\alpha}_s = (sign(\tau^s - x^s) - D\alpha^s)\dot{v}^s \;\; ; \;\; v^s = \int_0^t |\dot{\gamma}^s| \tag{3}$$

Homogenization was performed with the Beta-method [21], which allows to introduce self-consistent homogenization of different phase fractions and crystalline configurations without the need to compute large polycrystalline aggregates explicitly with a finite element (FE) mesh during parameter identification process. The method is presented in more detail in Appendix and here only briefly outlined. The models were then used in full field to perform the cleavage fracture related investigations.

The elastoplastic tensor $\underline{\beta}$ describes the interphase or intergranular constraints, i.e., the effect of other phases or grains. The module $\underline{\underline{L}}$ can be chosen in various ways, including Kröner's approximation, Eshelby's inclusion, or simply equal to the shear modulus of the material. The mean stress of a grain $\underline{\sigma}^g$ estimates the mean stress of a grain in a polycrystalline aggregate, that could also be solved with computationally more expensive FE discretization if numerical homogenization were to be utilized. $\underline{\sigma}^g$ is given by:

$$\underline{\sigma}^g = \underline{\Sigma} + \underline{\underline{L}}^g : (\underline{\beta} - \underline{\beta}^g) \tag{4}$$

The evolution of the accommodation tensor $\underline{\beta}$ can be written as [21]:

$$\dot{\underline{\beta}} = \dot{\underline{\epsilon}}_p^g - D^g \left(\dot{\epsilon}_p^{g,Mises} \left(\underline{\beta}^g - \delta^g \underline{\epsilon}_p^g \right) \right) \tag{5}$$

where D^g and δ^g are the scale transition parameters.

The FE meshes for CP modeling are constructed using image based modeling. In the approach the EBSD results are segmented based both on phase and orientation maps, and the resulting segmentation is used to assign meshing domains to identify all individual areas which yield differing local mechanical response. The image processing and meshing methodology is not presented in current paper in detail, but rather it is presented in [22,23] with respect to the basic approaches, and algorithmic background and applications to both 2D and 3D meshes showing typical parameterizations and applications for complex multimaterial domains are shown in [24,25].

2.4. The microstructure informed WST model

The WST model, as presented by the authors earlier in [8,9], is a cleavage fracture model that has been largely used to describe the scatter of fracture toughness and model the temperature dependency of fracture toughness of primarily ferritic and bainitic steels. The WST model is founded on a statistical cleavage fracture model identical to that of the Master Curve (MC) method (see, for example, [26]), and as such the self-similarity of a sharp crack stress–strain field is exploited. Whereas the MC method escapes the need for the exact quantification of the distribution of cleavage fracture toughness by the introduction of a 2–3 parameter Weibull like distribution, introducing the normalization fracture toughness K_0, the WST model aims at the accurate computation of the normalization fracture toughness. This is accomplished by explicit modeling of the local cleavage initiation and propagation probabilities. Otherwise the treatment of the probabilistic aspects of cleavage, arguments related to weakest link behavior and the whole underlying micromechanical model of cleavage fracture are in unison with the MC method and its derivations, which again have been illustrated to be in compliance with local approach (LA) models such as the modified Bordet model family or the MIBF model.

In the WST model, the conditional cleavage initiation probability is approximated by:

$$P_r\{I/O\} \approx \int_{d_c}^{\infty} P_{fr} \cdot (1 - P_{fr}) \cdot P_d \cdot \partial(d), \tag{6}$$

where P_{fr} is the failure probability for cleavage initiation, d_c is the critical initiator size, P_d the particle size distribution for initiators given as a function of d and $1 - P_{fr}$ stands for an approximation of survival failure probability. This stems from:

$$P_{fr}\{I/O\} = P_{fr}\{I\} \cdot \left(1 - P_{fr}\{V/O\}\right) \tag{7}$$

The conditional probability $P_{fr}\{V/O\}$ refers to void rather than cleavage nucleation for completeness of the probabilistic approach in describing the micromechanisms of cleavage (although the model as presented here accounts for effects associated with cleavage or void nucleation, limiting its ability to treat or incorporate any other mechanisms). The particle size distribution is adopted from [8,9] where it is presented as:

$$P_d = \frac{(\nu-2)^{\nu-1}}{\Gamma(\nu-1)} \cdot \left(\frac{d}{\bar{d}}\right)^{-\nu} \cdot \exp\left(-\frac{\nu-2}{\frac{d}{\bar{d}}}\right) \tag{8}$$

where ν is the distribution shape parameter, Γ the gamma function and $\bar{d}$ is the mean value of d. In current work the model is utilized to evaluate the cumulative fracture probability of the duplex microstructures based on post-processing of the CP modeled results, this development at present is referred to as the μWST model to reflect the difference. We utilize the model for the BCC phase of the ferrite–austenite steel, and in the classical WST model the local failure criterion is formulated by first defining the critical initiator cleavage driving stress as:

$$\sigma_p = \sqrt{\sigma_{yy} \cdot \varepsilon_{yy} \cdot 1.3 \cdot E_p}, \tag{9}$$

where σ_{yy} and ε_{yy} are the matrix material stress and strain state (typically opening or hoop ones) and E_p is the particle modulus of elasticity. The coefficient 1.3 results from earlier work [8,9] where the respective expression was develop to relate matrix stress–strain state to particle stress and the resulting form adopted. Particle response is considered similarly at present as in the classical model, i.e., isotropic and elastic constitutive response is assumed. In the present formulation, we replace this expression with its CP equivalents leading to particle cleavage stress expression of:

$$\sigma_p = \max\left|\sqrt{\left(\underline{n}_c^s \cdot \underline{\sigma} \cdot \underline{n}_c^s\right) \cdot \left(\underline{n}_c^s \cdot \underline{\varepsilon} \cdot \underline{n}_c^s\right) \cdot 1.3 \cdot E_p}\right|_c \tag{10}$$

where σ and ε are true stress–strain measures projected to cleavage planes c with a normal vector $\underline{n}^s$. In current work, the {100} cleavage planes of the BCC lattice and respective ferrite phase are considered (thus, at maximum a total of 6 cleavage planes per material point). This formulation follows the work carried out by the authors in [19,27]. The particle stress is linked to the failure probability of Eq. (7) by:

$$P_{fr} = 1 - \exp\left(-\left(\frac{d}{d_N}\right)^3 \cdot \left(\frac{\sigma_p}{\sigma_0}\right)^m\right), \tag{11}$$

where σ_0 and d_N are normalization parameters of the distribution and d is the initiator particle size as earlier.

Regarding the required WST model calibration, results presented for ferritic steels in earlier work [8,9] are used to infer effects of differing microstructural stress–strain states, especially as only very limited Charpy-V data is available for the present steels at present due to them being trial batches. This earlier work consists of baseline calibrations for the normalization parameters based on extensive experimental programs, and are considered sufficient for the preliminary investigations of the model performance as carried out presently. In current work, only the driving force as arising from microstructural stress–strain fields is investigated and updated, the model itself is to be further developed as a part of future work with respect to its parameterization for ferritic–austenitic duplex steels. Thus, in present work the data injected to the cleavage fracture model is informed of steel microstructure, and we refer to this implementation as the μWST model to separate from the earlier "top-down" micromechanical approaches with the similar modeling framework.

3. Results

We first present results with respect to principal characterization data, microstructures and their computational representation, followed up by calibration of the CP models. Followingly, the crystal plasticity model is utilized to investigate the deformation behavior of the dual phase ferritic–austenitic duplex steel microstructures. Firstly, we analyze the intra-grain and inter-grain stress states, local plastic strain accumulation and relate slip activity with stress build up in the microstructure. Secondly, in Section 3.5 continues to the assessment of the effective strain and stress distributions to the susceptibility of damage on the basis of using the proposed cleavage fracture model to assess the damage propensity of the banded and non-banded microstructures. Finally, in Section 3.6 we employ the established structure-properties-performance workflow for weakest link driven cleavage fracture to integrate a simple virtual design method to evaluate sensitivity of toughness to austenite morphology and volume fraction in ferritic–austenitic duplex steel microstructures.

3.1. Characterization

Three different methods were used to determine phase fractions of the studied steels as seen in Table 2. Steel C had the most austenite averaging 46%. In this case, Feritscope, Satmagan and EBSD were in good agreement. Measurement results between different methods in steels A and B were uncertain instead. In steel A, the result varied between 12.4 and 17.7% while in steel B, the amount of austenite was between 17.3 and 25.3%.

Microhardness of both ferrite and austenite were measured separately, as seen in Table 3. There was no significant difference on hardness of ferrite between the three steels. However, hardness of austenite ranged from 307 to 343 HV.

Table 3
Microhardness by phase [HV].

Steel	Ferrite	Austenite
A	247	343
B	253	333
C	253	307

Table 4
Tensile test results parallel to the rolling direction.

Steel	Rp0.2 [MPa]	Rm [MPa]	A5 [%]	Ag [%]	Rp0.2/Rm ratio
A	457	583	11.7	5.7	0.78
B	439	620	24.1	14.2	0.71
C	461	754	34.2	30.9	0.61

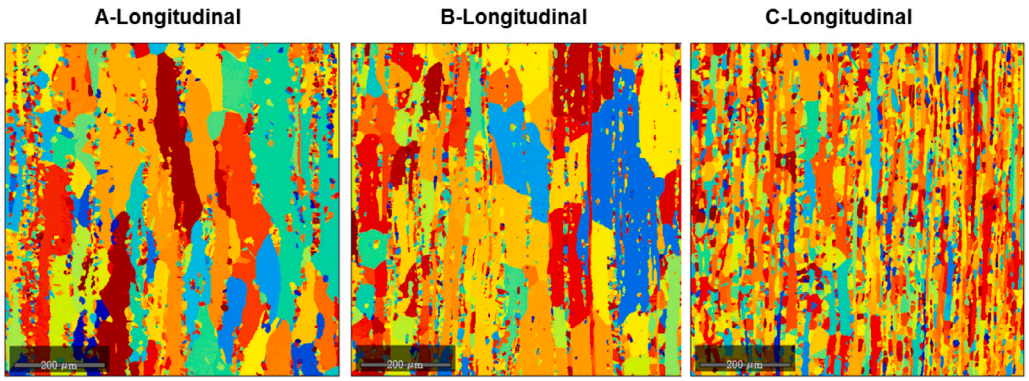

Fig. 1. EBSD inverse pole figure colored orientation plots of the three ferrite–austenite duplex steel microstructures: Longitudinal = in the rolling direction (vertical direction).

The tensile properties parallel to the rolling direction of the studied steels are given in Table 4. Yield stress (Rp0.2) and tensile strength (Rm) of the steels varied in the ranges of 439 to 461 Mps and 583 to 754 Mpa, respectively. Elongation to fracture (A5) varied from 11.7 to 34.2% while uniform elongation (Ag) ranged from 5.7 to 30.9%. The Rp0.2 to Rm ratios were in the range of 0.61 to 0.78.

3.2. Computational microstructures

Microstructures of the three investigated ferrite–austenite duplex steels are shown in Figs. 1 and 2. Material microstructures are characterized in the rolling and the transverse direction to incorporate the anisotropy of the microstructure in the following analyses. In Fig. 1 the inverse pole figure colored orientation plots of EBSD data are presented in the longitudinal direction relative to rolling. In Fig. 2 the microstructures are already segmented by phase and orientation to be used as direct input for model generation, i.e., this is the material microstructural geometry input for the FE model mesh generation. In this representation, typically larger ferrite grains as shown as darker gray, while austenite grains and banded austenite structure is show in lighter or nearly white coloring. Typical characteristics of the respective microstructures differ as a function of austenite fraction. For steel "A", the microstructure consists of large ferrite grains containing striations of small austenite grains. For steel "B", some austenite bands are seen embedded in the otherwise similar two phase microstructure. For steel "C", the ferrite and austenite fractions are similar and in the longitudinal direction a more typical duplex steel-like banded microstructure is witnessed.

The images of Fig. 2 are the direct input to the utilized meshing solution, and examples of subsequent FE meshes are presented in Fig. 3. The utilized methodology is able to resolve the finest details of the EBSD data, and the element characteristics are directly constrained by quality metrics imposed to the meshing algorithm. This eliminates problems arising from high element aspect ratios and distortions during the following FE solution. Due to the small polycrystalline features of the microstructure, the meshes were generated without any smoothing of the interfaces or iterative meshing practices, as it was desirable to ensure these characteristics were retained for following analysis of their respective effects. The behavior of the microstructures is investigated in uniaxial tensile loading. Regarding boundary conditions, the microstructures are constrained by kinetic-uniform boundary conditions (KUBCs), restricting the free edges transverse to loading direction to uniform displacement in their normal direction.

3.3. Crystal plasticity model parameterization

Fig. 4a presents an idealization of the Beta-method procedure for CP model calibration of the ferritic–austenitic duplex steels. Each steel was assigned phase fractions based on the microscopic determination of volume fractions. A total of 500 grains was used

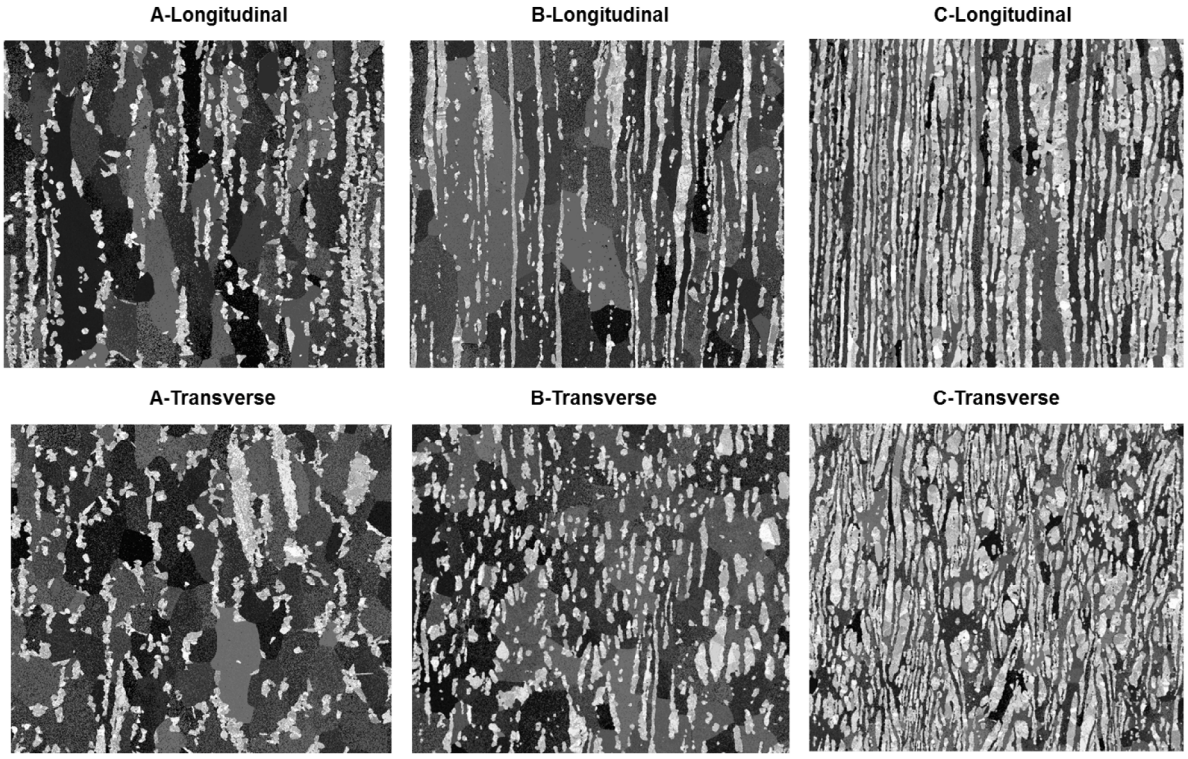

Fig. 2. Microstructures of the three ferrite–austenite duplex steels characterized in two perpendicular directions: Longitudinal = in the rolling direction and Transverse = transverse to the rolling direction.

Table 5
Single crystal parameters for the ferritic–austenitic duplex steels.

Parameter			
Elastic constants	Austenite	Ferrite	
C_{11} [MPa]	198 600	236 000	
C_{12} [MPa]	136 200	140 000	
C_{44} [MPa]	104 700	116 000	
Material	Steel A Austenite–Ferrite	Steel C Austenite–Ferrite	Steel B Austenite–Ferrite
Slip parameters			
τ_0 [MPa]	124.0–89.5	111.0–91.5	113.0–86.0
K [MPa $s^{1/n}$]	124.0–89.5	111.0–91.5	113.0–86.0
n	15.0–30.0	15.0–30.0	15.0–30.0
b	18.0–37.0	20.0–36.0	17.0–34.0
Q [MPa]	25.5–15.5	23.5–13.5	24.0–14.5
C	1000.0–1000.0	1000.0–1000.0	1000.0–1000.0
D	100.0–100.0	100.0–100.0	100.0–100.0
$h_1 - h_6(FCC)$	All 1.0		
$h_1 - h_8(BCC)$	All 1.0		
Scale transition			
D^g	300.0	300.0	300.0
δ^g	0.3	0.3	0.3

in each simulation. Fig. 4b–d shows stress–strain behavior of the three studied steels. Material parameter fitting was performed on strain rate jump tests to also capture strain rate sensitive behavior. Initial critical resolved shear stress values of each phase were linked to phase specific microhardness experiments. Lower strain rate sensitivity was assumed for the BCC phase (ferrite) as well as lower strain hardening capability. The simulated stress–strain responses reproduces the experimental curves with a decent accuracy in the range of simulated strains.

Table 5 collects the used single crystal parameters. Initial resolved shear stress ratio, i.e., yield stress ratio, between austenite and ferrite was initially set up based on hardness measurements performed on each phase. Elastic parameters for elasticity were not

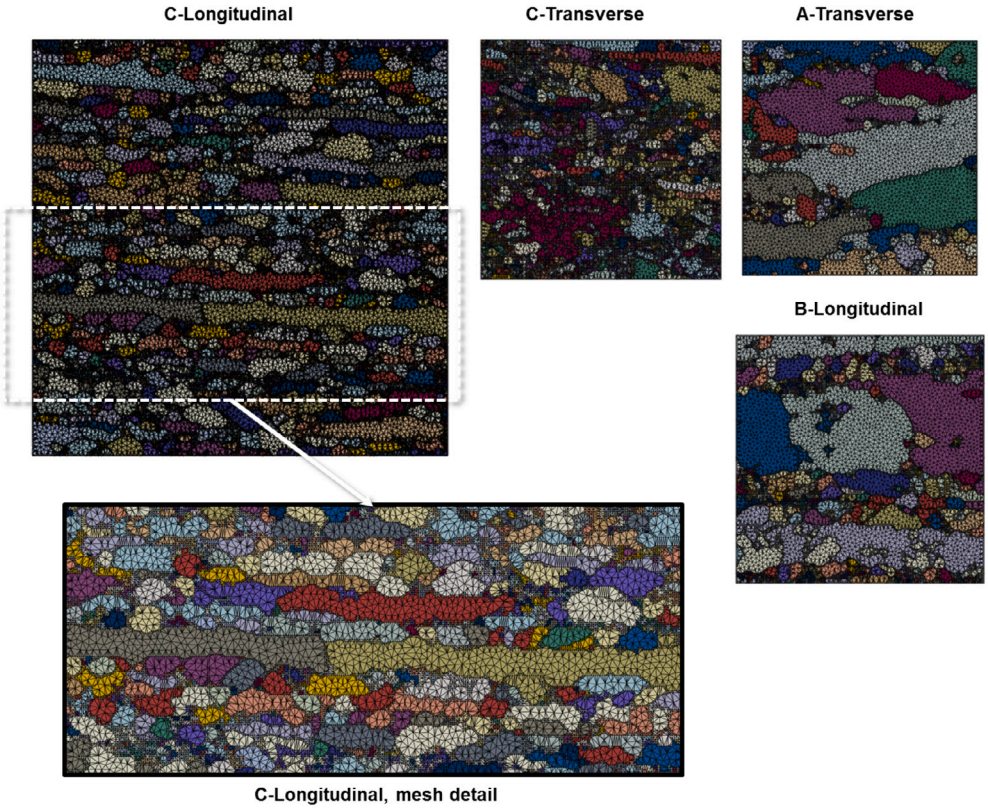

Fig. 3. Examples of finite element meshes for the different ferritic–austenitic duplex steels.

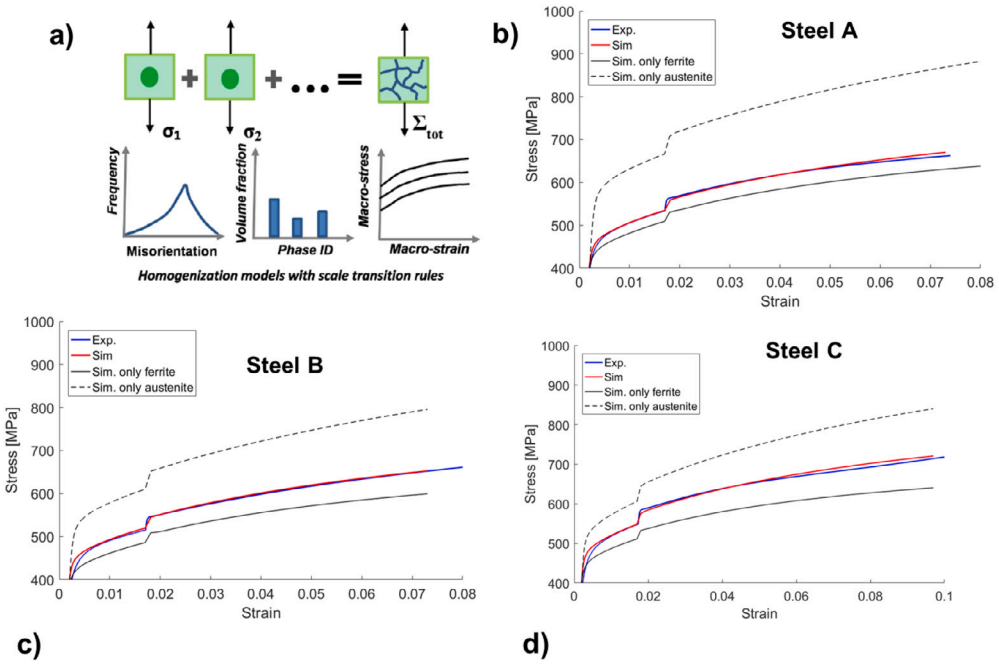

Fig. 4. Experimental and crystal plasticity simulated stress–strain curves with a strain rate jump for steels (a) schematic of the homogenization rule, (b) steel A, (c) steel B, and, (d) steel C.

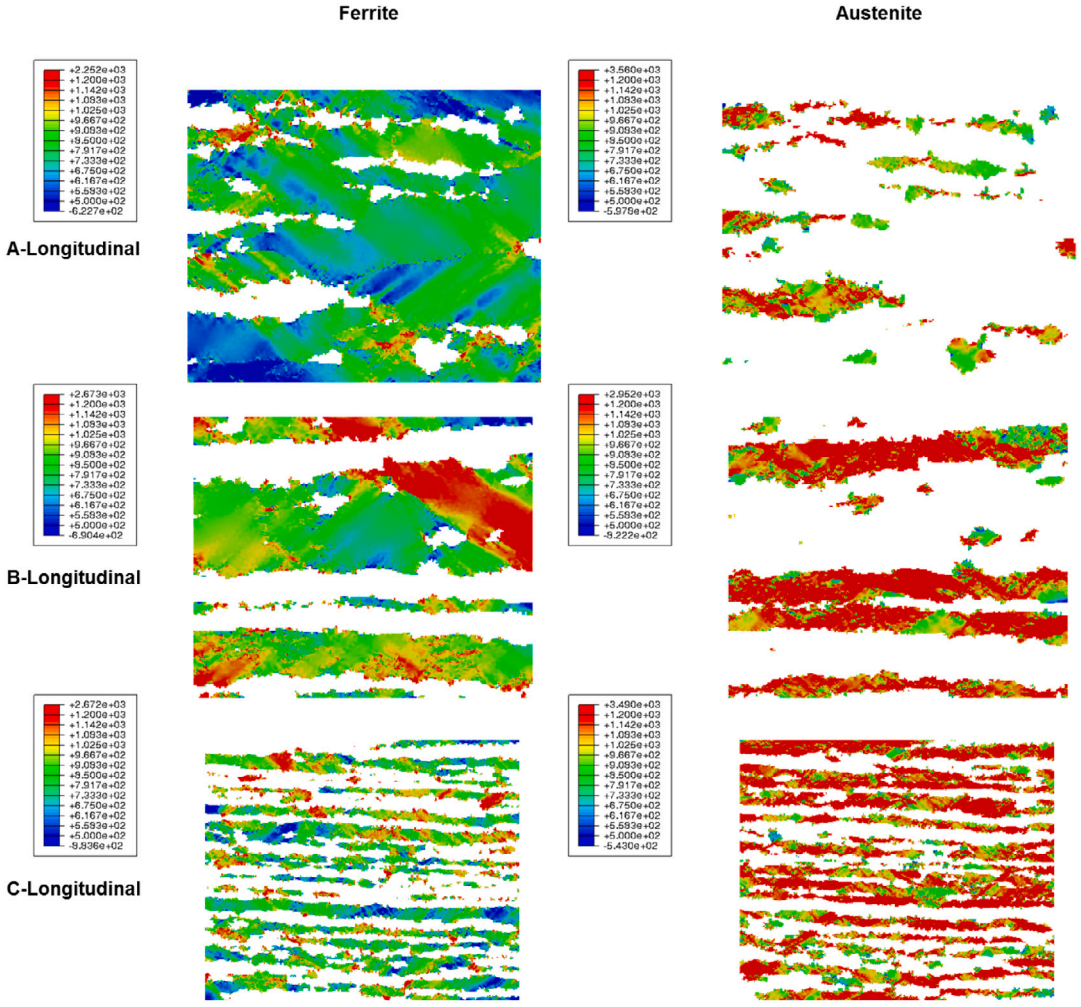

Fig. 5. First principal stress contours in ferrite and austenite phases of the studied steels under tensile loading (tensile direction horizontal).

part of the calibration but literature based values were used, following earlier work in [19]. The scale transition parameters related to self-consistent homogenization are further elaborated in Appendix.

3.4. Microscale deformation characteristics

Heterogeneity of stress and strain fields are witnessed for the three steel grades with varying microstructures with characteristics that can be correlated to grain and phase morphology, in the following the results are presented for 10% of tensile strain, which provides an overall view how the different structures exhibit plastic slip. In Fig. 5 the first principal stress contours of the three longitudinal microstructures are plotted, the results provided separately for the ferrite and austenite phases to ease interpretation of the results. For the "reference" ferritic–austenitic steel, steel C, it is seen that the higher strength austenite primarily shields the ferrite from higher tensile stresses, which would also be considered detrimental in terms of cleavage characteristics. Some local stress maxima are witnessed in the ferritic phase, these can be identified to relate to locally complex phase morphologies and favorably oriented grains relative to the applied tensile loading. No greater shear banding on indications similar slip localization across the phases are present. For steels A and B the behavior differs. For both steels the greater hardening of the austenite phase and its influence is still observed, however, due to the non-banded and discontinuous structure, the stress state within the ferrite differs. For steel A, some grains locally near larger regions of austenite are seen to exhibit tensile stress maxima. For steel B, where in this microstructure coarser austenite bands split the ferrite phase, it is observed that some of the very coarse grains develop high tensile stress states as well.

Regarding cumulative plastic slip, presented in Fig. 6 for Steels B and C (results for steel A are similar to steel B), differences between banded and non-banded structures arise (particularly as the tensile loading is being applied via a uniform strain boundary condition). With respect to steel B with its smaller austenite phase fraction and larger ferrite grain size, the ferrite phase allows for

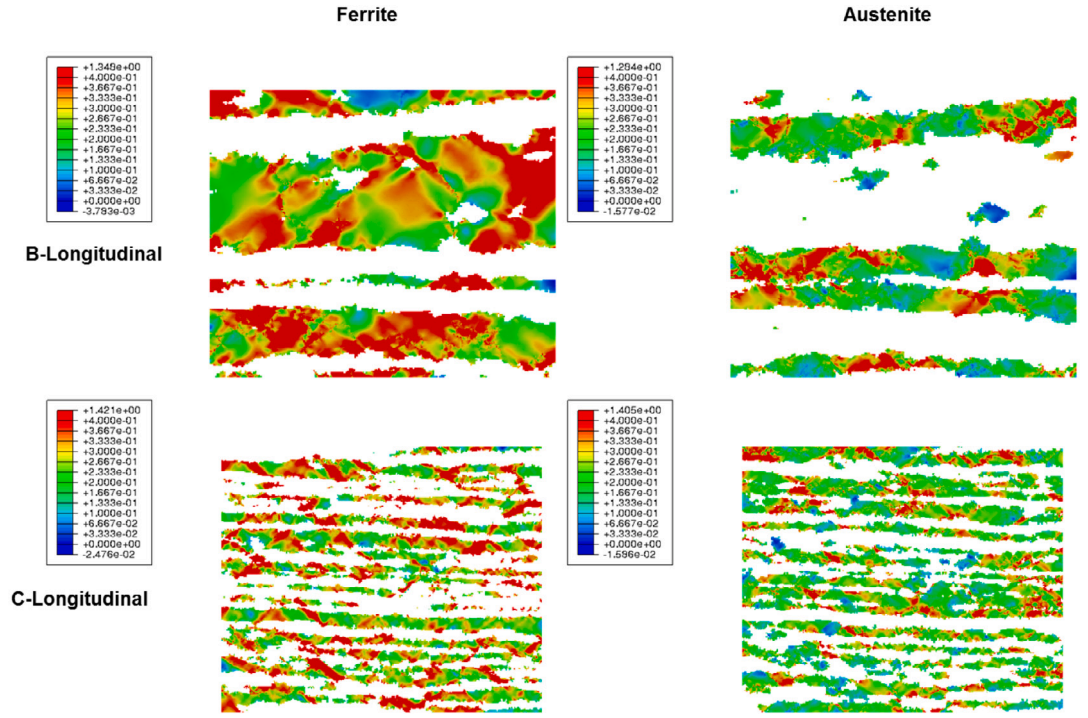

Fig. 6. Cumulative plastic slip contours in ferrite and austenite phases of steels B and C in longitudinally oriented microstructure under tensile loading (tensile direction horizontal).

more inter-grain transmission of shear deformation which propagates across several larger grains in some instances. The austenite phase show signs of high activity of slip in some grains, that are favorably oriented, while other regions effectively arrest the development of the ferrite based shear banding. Larger effective grain size of steels A and B and the somewhat lower strength ferrite phase opens up deformation pathways supported by the lack of larger continuous austenite bands in the microstructure. Plastic strain can then accumulate and the mismatch supports the formation of larger plastically deforming regions in both phases.

The differences between longitudinal and transverse microstructures can be assessed based on results presented in Fig. 7 for steel B. Overall and in qualitative terms in comparison to the longitudinal results, it can be argued that the findings are quite similar with respect to the behavior of the larger ferrite grains, both regarding the first principal stress distribution and cumulative plastic slip accumulation. The ferrite phase shows locally high values of first principal stress, arising from interaction of the austenite phase. The larger ferrite grains, similarly to the longitudinal direction, exhibit concentration of plastic slip beyond what is witnessed for the banded ferritic–austenitic microstructures in extent and magnitude of the values.

3.5. Cleavage stress–strain state and failure probability

The cleavage fracture failure probability, as expressed in Eq. (11), can be directly computed based on crystal plasticity modeling results. The approach was to assess different plausible initiation sites and evaluate the respective failure probability within the microstructure. The possible initiation sites are all the ferritic phase material points in the FE solution. The dominating one, the weakest link, would then prove to be the one critical with respect to initiation of the cleavage fracture. The failure probability, P_{fr}, can be linked to the Master Curve normalization fracture toughness, K_0, as presented in [8] and further utilized to assess the median fracture toughness, K_{Jc}, following the standard Master Curve analysis procedures as in [26]. With respect to cleavage fracture process zone, a convention adapted also in previous work was utilized, i.e., the zone is considered to extend to the local plastic zone. The analyses are performed as a function of applied loading and in some cases also for different temperatures, this in order to obtain crude estimates of the fracture toughness transition adequate for the purposes of present work (utilizing analysis approaches regarding the fracture mechanical treatment and respective material and model properties as presented previously by the authors in [8,9,26]). In the case of different temperatures the crystal plasticity model is used in a temperature dependent manner.

Example how the model data is treated and how do differences between the microstructures appear is presented in Fig. 8. For the banded microstructure, steel C, it is noted that the probability density function (PDF) overall covers lower values than for steel A, implying better performance against cleavage fracture. The different regions containing local stress concentrations of steel A are emphasized in Fig. 8. The maxima within the ferritic phase are indicative of likely cleavage initiation sites, and within the microstructure, they relate to locations of large ferrite grains adjacent to small austenite grains. This yields a situation where

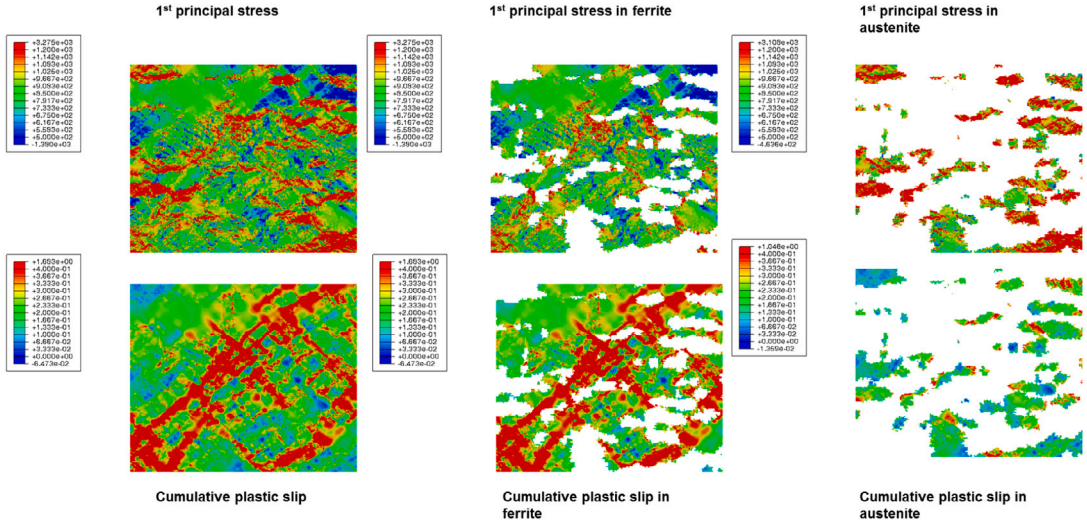

Fig. 7. First principal stress and cumulative plastic slip contours in steel B for transversely oriented microstructure under tensile loading (tensile direction horizontal).

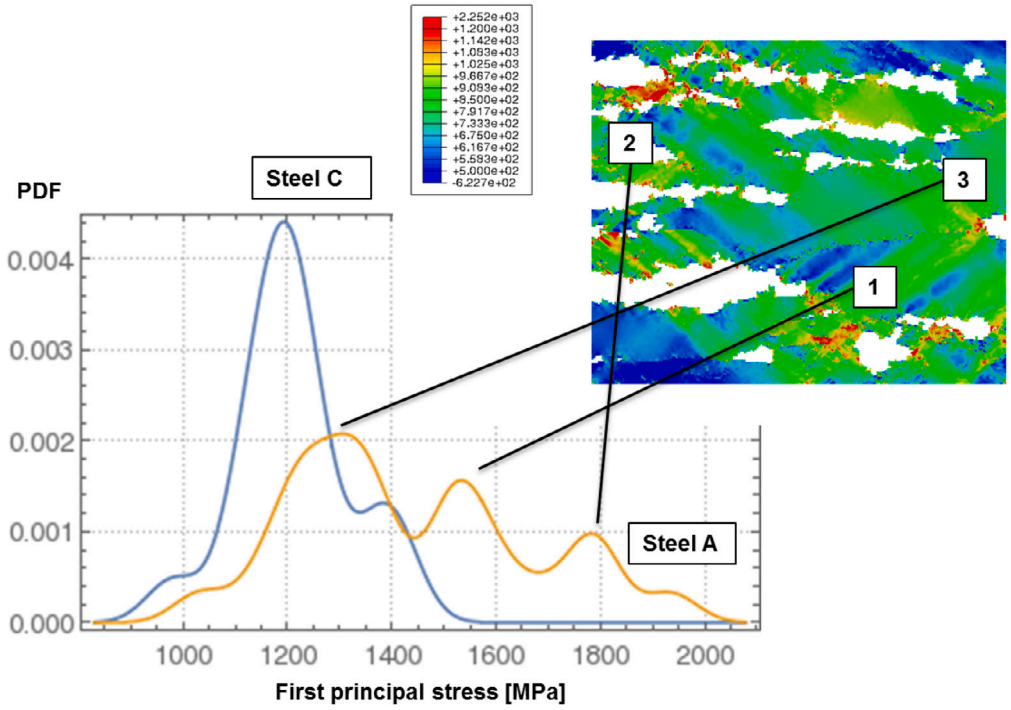

Fig. 8. Probability density distribution of stresses in the ferrite phase in steel A with non-banded microstructure vs steel C with banded microstructure.

the property (hardening) mismatch between the phases drives the increase of stress further promoted by slip localization in the ferritic grains. With respect to indicative detrimental effects in steels A and B vs. steel C this appears to be the primary mechanism, particularly, when the local maxima in both cleavage driving stresses and plastic slip exceed those of the banded structure.

How the stress–strain state reflects upon cleavage initiation probability is presented in Fig. 9. The different curves correspond to different local maxima in the microstructure which can act as possible cleavage initiation sites. Similarly and as indicated by the results pertaining to microstructural stresses and plastic slip, it is noted that the calculations imply the banded structure is more efficient in retarding cleavage initiation than the non-banded one containing only separate and non-connected austenite regions.

Calculation of the failure probabilities persistent to specific maxima in the microstructure provides one with the means to assess fracture properties of such an RVE. Thus, for a single temperature a fracture toughness estimate can be obtained, when

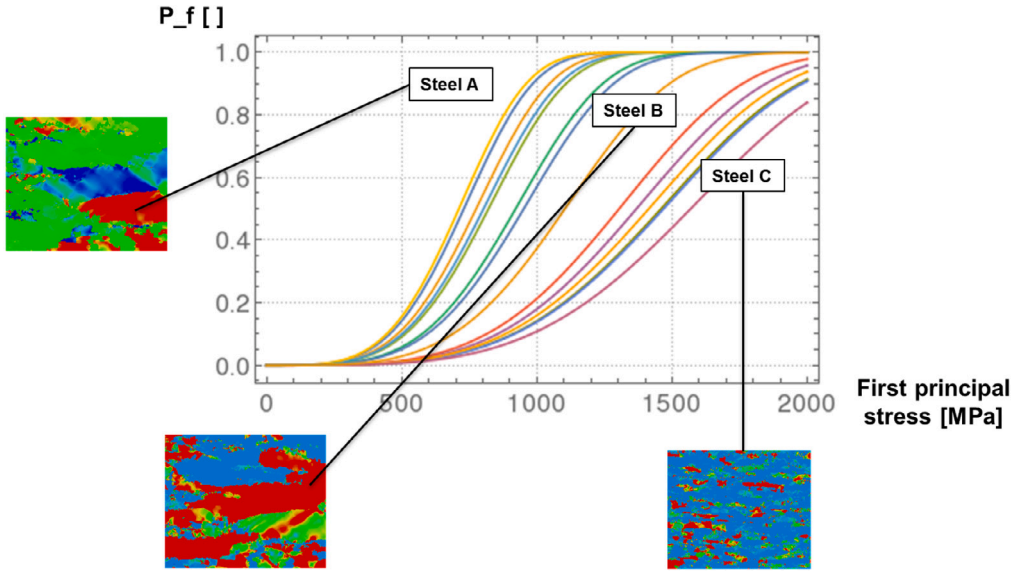

Fig. 9. Computation of cleavage failure probability as a function of first principal stress for the different steels.

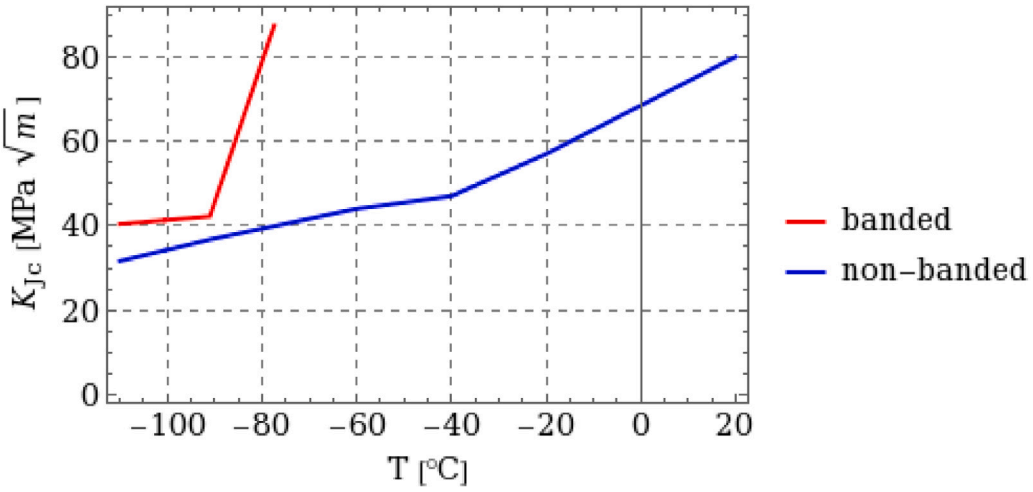

Fig. 10. μWST based representation of the ductile-to-brittle transition region fracture toughness for banded and non-banded (steel B) ferritic–austenitic microstructures.

the analysis is repeated across temperatures of the ductile-to-brittle transition (DBT) region fracture toughness prediction can be obtained. The assessment when carried out for three different temperatures per microstructure (−110 °C, −90 °C, −40 °C, 20 °C, different temperatures for different microstructures and the respective properties adopted from [8,9,26]) is presented in Fig. 10. The assessment methodology supports, as expected based on previous results, the notion that the cleavage characteristics of the banded microstructure exceed those of the non-banded one. Of particular significance is of course the result itself, i.e., the proposed approach enables one to systematically link microstructural features to a complex material property, the cleavage fracture toughness. Further analysis on how the results are comparable to experimental findings is provided in the discussion section.

3.6. Synthetic multi-phase microstructure design against cleavage fracture

In order to further investigate the fracture toughness ferritic–austenitic microstructure dependency as well as evaluate possibilities in exploiting the presented micromechanical modeling methodology, few simple synthetic microstructures were generated and the developed cleavage fracture toughness model applied to investigate and predict the resulting fracture toughness response. Since the motivation for current work has been to investigate whether non-banded ferritic–austenitic duplex steel microstructures could be exploited with less austenitic phase (and as such, simpler alloys) with a favorable phase morphology (spherical and

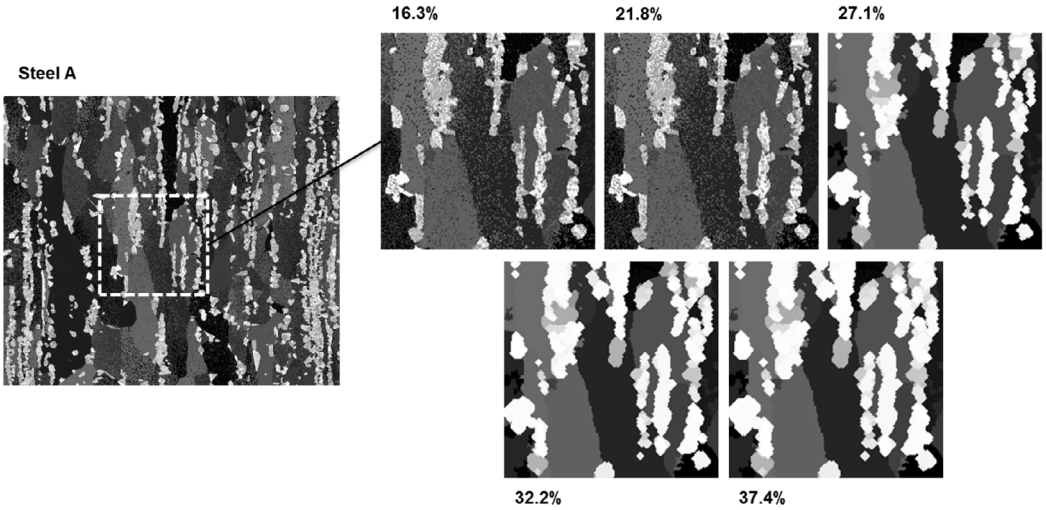

Fig. 11. Synthetic microstructures based on Steel A with different austenite phase fractions from the original 16.3% to 37.4%.

rounded regions of austenite), the approach selected was to increase the austenite phase fraction by dilating the respective individual grains "embedded" in the ferrite phase. This enables one to initiate the analysis based on existing microstructures, and then assess systematically how the stress–strain fields contributing to cleavage fracture probability evolve as a result. Modified microstructures based on Steel A are presented in Fig. 11, the increases in austenite phase fraction were motivated in part by the range which would be expected to demonstrate the benefits of the selected strategy with respect to the resulting cleavage fracture behavior.

The influence to local stress-plastic slip state within the ferrite phase is presented in Fig. 12 for three different austenite phase volume fraction, two in addition to the original one for Steel A. The locations of first principal stress maxima at different microstructures are indicated and the numerical PDF is plotted for the three phase fractions. Regarding cumulative plastic slip, the primary behavior of large ferritic grains is retained when an increase in the phase fraction of only some 15% is considered. Some smoothening of slip bands near concentrations of plastic strain is seen, but the effects in current case are evidenced particularly in the homogenization of the first principal stress distribution. The maximum stresses located at morphologically complex microstructural locations are seen to smoothen out a somewhat, this is particularly visible from the plotted PDF distributions. The increase in austenite phase fraction cuts off the peak stress values some 200–400 MPa, and overall scales the distribution towards smaller values. This can be argued to be the effect sought with the increase of the austenite phase fraction, i.e., the propensity of the ferrite phase to nucleate cleavage damage can be argued to have been decreased a somewhat.

The quantitative impact to fracture toughness can be estimated using the μWST model following the same workflow as previously. The results are presented in Fig. 13 as fracture toughness DBT curves. The different modified microstructures and their results are presented as a single set of fracture toughness transition curves. It is seen that the behavior of the banded ferritic–austenitic microstructure is still not within reach with the present strategy, but a fracture toughness transition temperature T_0 improvement of roughly 40 °C might be obtainable. The comparability of these observations to common experimental findings is discussed in more detail in the following sections.

4. Discussion

4.1. Effect of alloying and phase morphology on microstructural plastic slip

Dissimilarities between amount of austenite in different steels depended directly on volume of austenite favoring alloying elements, namely Ni and Mn. Thus, the highest amount of austenite was formed in steel C. Uncertainty of amount of austenite in steels A and B can be explained in following way: the samples for Feritscope and Satmagan were prepared using mechanical polishing, which considering the metastability of the austenite phase can as a result yield a degree of scatter. On the contrary, the samples for EBSD were electropolished thus being free of any deformation affecting the studied surface. Hence, the amount of austenite on steels A and B was relatively higher measured with EBSD in comparison to Feritscope and Satmagan. However, the differences were minor enough not to result in any direct challenges with respect to model parameterization by way of self-consistent modeling of the ferritic–austenitic microstructure, and overall, it can be argued that the full field analyses with complete microstructural models are not influenced.

In the current studied ferritic–austenitic duplex steels the austenite phase has greater strength over the ferritic one. This influences the basic plastic deformation behavior of all the studied steels. The calibration using the multi-phase CP model was found more than able to match the available experimental information, including indirect observations via local microhardness values, and as such, the findings can be considered more than indicative. Also, characteristics such as microhardness were found not to reflect

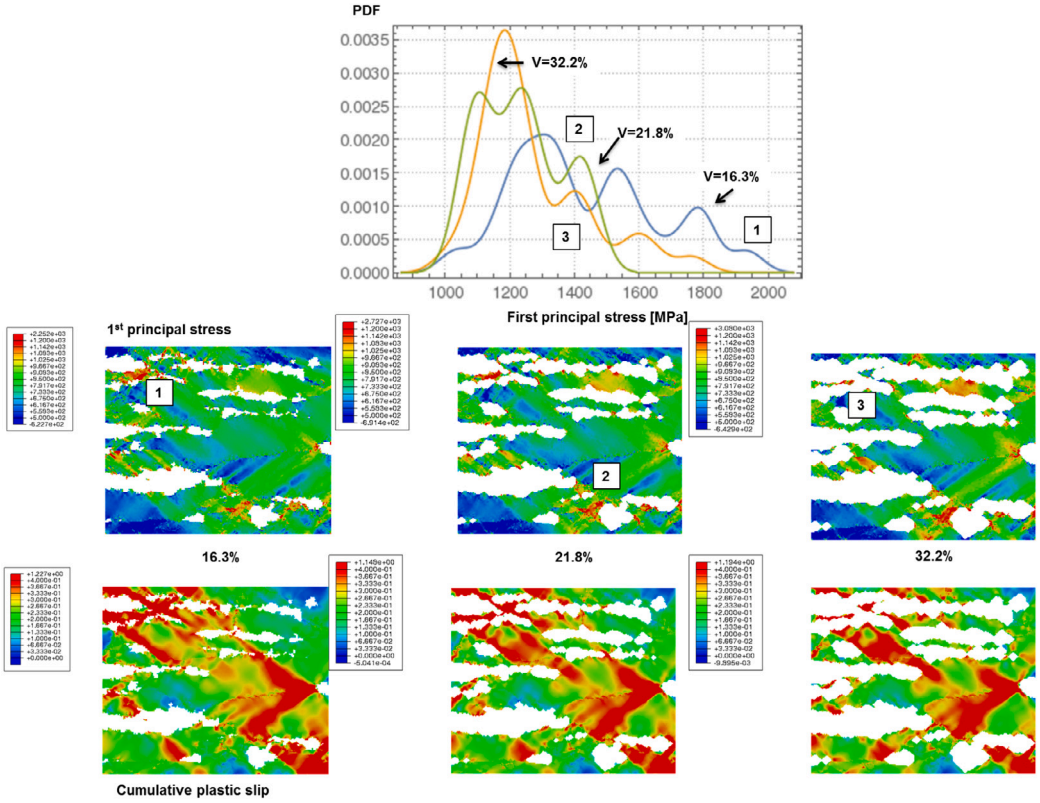

Fig. 12. First principal stress and cumulative plastic slip contours on synthetic microstructures based on Steel A with different austenite phase fractions from the original 16.3% to 32.2% (tensile direction horizontal).

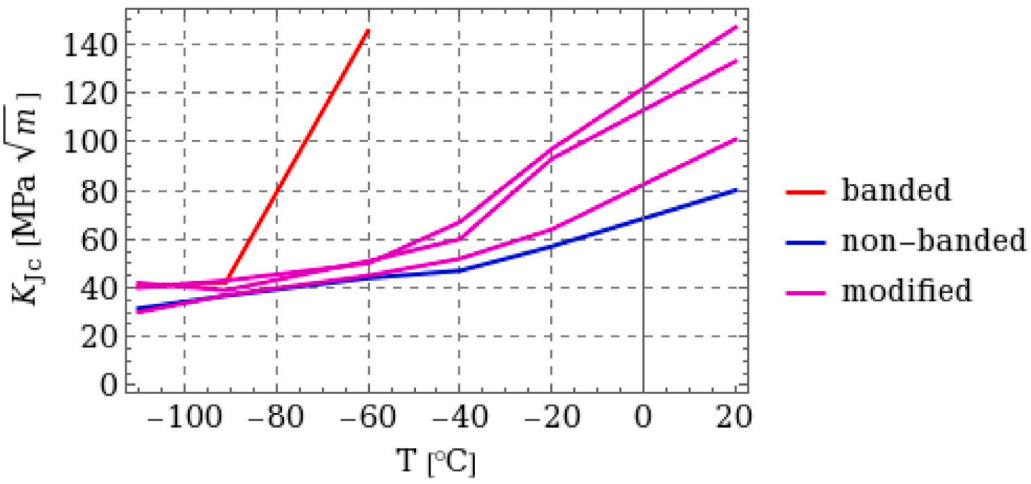

Fig. 13. Synthetic microstructures and fracture toughness predictions for the ductile-to-brittle transition region and comparison to banded and original non-banded microstructures.

characteristics such as ferrite grain size, further eliminating sources of doubt. The question regarding TRIP behavior is discussed below in the context of further developing CP models for dual phase, duplex-like, steels.

The stress-plastic slip response of the microstructures was, in addition to the austenite vs. ferrite strength aspect as emphasized below, found to be particularly dependent on the following features, with emphasis on characteristics influencing cleavage initiation. Firstly, the greater strength and hardening of the austenite phase does promote stress concentration in the ferrite phase. This effect is subtle, but the adjacent ferrite grains suitably oriented with respect to applied loading respond by developing higher tensile stress

states. Identically, in order to do so and retain compatibility large local plastic slip, also slip bands, evolve in the ferrite grains. These features were found to be emphasized by locally complex morphologies, for example, very small austenite grains embedded among large ferrite grains. The large ferrite grains themselves promote slip localization arising from the aforementioned features, and there were several instances where near grain boundary regions of large grains exhibited significant plastic slip in the non-banded microstructures.

4.2. Micromechanisms of failure and fracture toughness

The numerical results suggest differing failure micromechanisms for the non-banded and banded ferritic–austenitic duplex steel microstructures, both regarding initiation and propagation, the latter not explicitly treated within the confines of the current work. Further propagation associated mechanisms would be rather linked to mechanisms like crack bridging, shielding and branching in multiphase microstructures arising from the fundamentally different toughness responses of the austenitic and ferritic phases. The cleavage fracture models and micromechanical understanding of the mechanisms of cleavage damage initiation point to a weakest link mechanism (as in [26], for example, and numerous related works). Thus, the local differences in stress–strain state, or cleavage stress and plastic slip, are dominating. On this basis, the micromechanical modeling results can be interpreted as such that the nucleation mechanism in the ferritic phase is associated with the cleavage stress increase from the ferrite–austenite mismatch and especially on the slip localization taking place in larger ferritic grains adjacent to any grain boundaries. Overall we can argue that this is in line with typically cleavage fracture mechanisms witnessed in ferritic–austenitic duplex steels, where regarding initiation the development of stress–strain state locally within the ferrite phase is responsible for cleavage initiation (elaborated in more detail immediately below).

In terms of these observations comparing to the cleavage behavior of duplex steels, some general observations can be already made based on earlier studies. The fracture characteristics, i.e., the role of austenitic bands and the morphology of the ferrite is in line with traditional, “classical” banded ferritic–austenitic duplex steels, as experimentally investigated, e.g., in [28]. Also, the deleterious effects to toughness follow the same micromechanisms based logic, which for more classical duplex steel grades has been investigated by several researchers, as in [29–31]. These works also acknowledge the role of microstructural morphology in the resulting fracture appearance and as such are principally in line with the investigations and approach of current work, and the argumentation regarding the role of the ferrite phase in terms of cleavage initiation and propagation holds, as well as the interactions during damage evolution and plasticity arising from the multiphase structure. The observations of current work and analyses of local fracture behavior and the role of different phases, as in [32], are in line with the present interpretation of the micromechanisms also from a fracture micromechanical perspective. In current work, the behavior in comparison to the most typical ferritic–austenitic steels differs due to the morphological characteristics of the non-banded microstructures. As a follow up, dedicated fracture toughness tests are planned to support further model development and the taking of more quantitative steps towards validation.

With respect to improvement in fracture toughness, there are, for example, aspects which we can argue would result in improvement in the fracture toughness of the non-banded microstructures, if the improvement of fracture toughness with fairly low austenite phase fractions is made a priority. One is to try to change the austenitic phase morphology. In the current microstructures, the spherical or rounded-like regions with smaller grains do not work quite optimally. Features with greater aspect ratio, smaller microstructural bands, would be more efficient in not promoting slip localization in the ferrite phase but with suitable sizing relative to the ferritic features would contribute to strengthening while being more efficient in limiting the initiation of cleavage damage. With respect to crack propagation, ductile bands embedded in the microstructure with similar phase fractions would be expected to work more efficiently. Another deleterious feature are the large ferrite grains, these are harmful regarding cleavage initiation both with respect to limiting plastic slip and increasing the cleavage driving stress state before initiation, and also, for increased plastic deformation localize the slip promoting cleavage fracture, especially one which follows ductile crack initiation. Still another feature are the differences in grain sizes between the austenitic and ferritic phases, the small grain size of austenite does add to the mismatch of the microstructure in carrying a stress–strain state, and while this can be argued to be a secondary feature in the current microstructures, it is a feature to address within the realm of processing options for improved behavior of the microstructures at conditions pertinent to cleavage fracture.

In terms of modern Integrated Computational Materials Engineering (ICME) principles for steels, current work focuses rather on the structure–property causal relations and correlations. A prudent way forward would be to incorporate processing aspects in more detail, either via addressing experimental process windows, statistical models or specific modeling of the manufacturing related deformation, solidification and heat treatments, as in the context of ICME by the present authors has been performed in [33,34] and will be considered a future work item. However, what even the present work based on imaging-based modeling of microstructures presents is that the merger of these kinds of experimental and modeling activities as workflows is an effective means to systematically track such causalities, already providing a tool for the design of complex microstructures, processing and alloying of steels.

4.3. Crystal plasticity and fracture modeling of duplex steels

The focus of current work was in addressing the basic deformation mechanisms in ferritic–austenitic duplex steels as evidenced by CP modeling and implications to cleavage fracture initiation. The methods and constitutive models can and are foreseen to require and see further development to increase their realism in the future.

A major contributor to strengthening of the dual phase steels can be sought by utilizing austenite phase metastability towards optimized material solution, i.e., strengthening arising from transformation-induced plasticity (TRIP). Transformation from austenite to martensite is a known strength–ductility attribute in the design space of transformation plasticity steels. Present results demonstrate the effectiveness of the micromechanical approach on establishing relationships between microstructure and performance in computationally robust manner. This is a characteristic which has not been addressed in fracture property related papers and is a point of further work current authors have pursued with the development and calibration of the respective constitutive models in [20]. Integration of TRIP effects and austenite stability when targeting improved fracture performance is a clear route for further computational research. Similarly, improved treatment of size effects by higher order plasticity models are an aspect to pursue, as in, for example, [17,27] for primarily ferritic-like BCC microstructures. These are foreseen to improve the capability to modeling to address the features highly difficult and laborious to consider experimentally.

Furthermore, CP modeling can be a beneficial tool to estimate the effects of phase transformations to the material performance. The performance predictions can be carried out either with the use of the present indicator based model (post-processing like estimation of fracture associated parameters, as in [8,9]) or more detailed micromechanical damage modeling approaches (as in [17–19]). Microstructure level damage modeling for single and multiphase steels is an attractive field of study to further assist faster development of new material solutions. Coupling transformation plasticity and evolution based damage is a challenging scope because of the possible failure initiation in multiple phases, including austenitic and several ferritic phases, all requiring a treatment of suitable crystalline damage mechanisms. The assessment of brittleness of newly formed martensite due to phase transformation is an intriguing aspect for the CP damage models. Recent work referred to above on transformation assisted plasticity with damage evolution has shown prominent possibilities in interfacing complex strain hardening mechanisms with crystalline level damage. Similar approach could be considered for the present materials as well and are an evident way forwards evaluating and exploiting the respective micromechanical phenomena.

Another challenge is the parameterization of the fracture models, such as the WST and the μWST variant. In principle we can separate, for the sake of discussion, three approaches. The present ‘‘engineering solution’’ largely employed by the community is the utilization of macroscopic test data, such as fracture toughness tests, reproduce these and by way of classical homogenization extract calibrations and parameter sets. With respect to temperature dependencies of the parameters, various authors have acknowledged the problem and presented differing solutions, see, e.g., [35–37] for various engineering ways to tackle the problem. Such works have improved upon the usefulness of the respective models, although not fully resolving the underlying micromechanics in terms of capturing the respective physical phenomena. Another way is to employ multiscale modeling and by way of adding to the mechanistic interpretation of the fracture process further the extraction of workable parameter sets. The likely best practice in terms of getting forwards is to supplement the second option, and as such add to its capabilities in describing failure processes in actual engineering materials, by smaller scale micromechanical and in-situ tests. Direct observations and their reproduction by models at the respective scales can be argued to yield more consistent and unequivocal parameter sets, and speed-up and reduce the effort in establishing the respective information to be utilizable. Current work is somewhere between the first and third options, the basic parameter set traced to [8,24] houses small scale data, but also, traditional fracture toughness DBT tests the applicability of which has been extended here to study the trends in fracture toughness as dependent on microstructural stress–strain states.

5. Summary and conclusions

Crystal plasticity modeling of image-based ferritic–austenitic duplex steels microstructures was carried out. In addition, micromechanical modeling of cleavage fracture initiation was performed with a derivative of the original WST model, the so called μWST model. The results of this work can be concluded as follows:

- The multi-phase crystal plasticity implementation was found able to reproduce the available experimental data based on macroscopic tensile data when constrained by local microstructure scale measurements.
- The imaging-based full-field microstructural analyses demonstrated the significance of microstructure features, such as austenite-to-ferrite phase fraction, ferrite grain size and morphology of austenite with respect to the resulting stress–strain state and evolution of plastic slip.
- Regarding cleavage fracture initiation, it was found that the reduction of austenite phase fraction and differences in austenite morphology from banded to non-banded resulted in increase of local plastic slip and cleavage fracture stress promoting cleavage failure. Microstructural features such as the large ferrite phase grain size were found to further weaken the characteristics attributable to improved fracture properties.
- Further developmental needs were identified and are being pursued, related to, for example, the inclusion of transformation-induced plasticity and fully coupled damage accumulation when modeling cleavage fracture initiation, propagation and the role of ductile initiation behavior preceding brittle fracture.
- The use of synthetic microstructures appears a viable means to further improve upon the exploitability of micromechanical modeling. In current work, simplistic work performed simply with phase fractions already provided insights as to the structure–property relationship related to cleavage fracture initiation.

Declaration of competing interest

The authors declare that they have no known competing financial interests or personal relationships that could have appeared to influence the work reported in this paper.

Acknowledgments

This study has been carried out as part of the Finnish joint industrial consortium research action coordinated by DIMECC Ltd within the BSA Breakthrough Materials program in the FUNMODE project. We gratefully acknowledge the financial support of Business Finland (formerly Tekes), the participating companies, and VTT Technical Research Centre of Finland Ltd. AL wishes to acknowledge the support of Academy of Finland through the HEADFORE project, Grant No. 333226. SU acknowledges Jenny and Antti Wihuri Foundation and Tauno Tönning Foundation for their financial support.

Appendix. Self-consistent homogenization using the Beta-method

The Beta-method [21] was utilized in performing self-consistent homogenization of the different phases and crystal plasticity configurations. The reasoning for the use of the Beta-method is to improve upon the computational efficiency of the calibration process and make it easier to obtain representative results. The latter arises from the low cost in the inclusion of a large number of orientations in the self-consistent approach.

The utilized scale transition rule is summarized briefly below. The $\underline{\sigma}^g$ estimates the mean stress of a grain in a polycrystalline aggregate. This could also be solved with computationally more expensive FE discretization if numerical homogenization were to be utilized. The mean stress $\underline{\sigma}^g$ is given by:

$$\underline{\sigma}^g = \underline{\Sigma} + \underline{\underline{L}}^g : (\underline{\beta} - \underline{\beta}^g) \tag{12}$$

where $\underline{\Sigma}$ is the macroscopic stress and $\underline{\underline{L}}^g$ is the material module. The elastoplastic tensor $\underline{\beta}$ describes the interphase or intergranular constraints, i.e., the effect of other phases or grains, and is given by:

$$\underline{\beta} = \langle \underline{\beta}^g \rangle = \sum_{g=1}^{N_g} f_g \beta^g \tag{13}$$

where the volume fraction of a phase g is denoted by f_g and the number of phases as N_g. The module $\underline{\underline{L}}$ can be chosen in various ways, including Kröner's approximation, Eshelby's inclusion, or simply equal to the shear modulus of the material (see [21] for more details). The evolution of the accommodation tensor $\underline{\beta}$ can be written as [21]:

$$\dot{\underline{\beta}}^g = \dot{\underline{\epsilon}}_p^g - D^g \left(\dot{\epsilon}_p^{g,Mises} \left(\underline{\beta}^g - \delta^g \underline{\epsilon}_p^g \right) \right) \tag{14}$$

where D^g and δ^g are the scale transition parameters of [21] and $\dot{\epsilon}_p^{g,Mises}$ is the rate of local viscoplastic deformation. The criteria for these parameters during the optimization process is that the self-consistency criterion needs to be met as $\underline{E} = \langle \underline{\epsilon}^g \rangle$ between the macroscopic and local strains.

References

[1] Gunn R. Duplex Stainless Steels : Microstructure, Properties and Applications. Cambridge: Abingon Publishing; 1997.
[2] Guo Y, Sun T, Hu J, Jiang Y, Jiang L, Li J. Microstructure evolution and pitting corrosion resistance of the Gleeble-simulated heat-affected zone of a newly developed lean duplex stainless steel 2002. J Alloys Compd 2016;658:1031–40.
[3] Papula S, Anttila S, Talonen J, Sarikka T, Virkkunen I, Hänninen H. Strain hardening of cold-rolled lean-alloyed metastable ferritic-austenitic stainless steels. Mater Sci Eng A 2016;677:11–9.
[4] Herrera C, Ponge D, Raabe D. Design of a novel Mn-based 1GPa duplex stainless TRIP steel with 60% ductility by a reduction of austenite stability. Acta Mater 2011;59(11):4653–64.
[5] Uusikallio S, Jaskari M, Kisko A, Nyo T, Porter D, Kömi J. Sample preparation challenges with highly metastable ferritic-austenitic stainless steels. Practical Metallogr. 2019;56:373–92.
[6] He J, Piao Z, Wang X, Lian J, Münstermann S. Micromechanical modeling of cleavage fracture for a ferritic-pearlitic steel. Eng Fract Mech 2019;221:106683.
[7] Kunigita M, Aihara S, Kawabata T, Kasuya T, Okazaki Y, Inomoto M. Prediction of Charpy impact toughness of steel weld heat-affected zones by combined micromechanics and stochastic fracture model – Part I: Model presentation. Eng Fract Mech 2020;230:106965.
[8] Wallin K, Laukkanen A. New developments of the Wallin, Saario, Törrönen cleavage fracture model. Eng Fract Mech 2008;75(11):3367–77, Local Approach to Fracture (1986–2006): Selected papers from the 9th European Mechanics of Materials Conference.
[9] Wallin K, Laukkanen A. Aspects of cleavage fracture initiation – relative influence of stress and strain. Fatigue Fract Eng Mater Struct 2006;29(9–10):788–98.
[10] Boåsen M, Stec M, Efsing P, Faleskog J. A generalized probabilistic model for cleavage fracture with a length scale – Influence of stress state and application to surface cracked experiments. Eng Fract Mech 2019;214:590–608.
[11] Ruggieri C, Dodds RH. A local approach to cleavage fracture modeling: An overview of progress and challenges for engineering applications. Eng Fract Mech 2018;187:381–403, SI: 50th Anniversary Issue.
[12] Forget P, Marini B, Vincent L. Application of local approach to fracture of an RPV steel: effect of the crystal plasticity on the critical carbide size. Procedia Structural Integrity 2016;2:1660–7, 21st European Conference on Fracture, ECF21, 20-24 June 2016, Catania, Italy.
[13] Libert M, Rey C, Vincent L, Marini B. Temperature dependant polycrystal model application to bainitic steel behavior under tri-axial loading in the ductile–brittle transition. Int J Solids Struct 2011;48(14):2196–208.
[14] Kim E-Y, Woo W, Heo Y-U, Seong B, Choi J, Choi S-H. Effect of kinematic stability of the austenite phase on phase transformation behavior and deformation heterogeneity in duplex stainless steel using the crystal plasticity finite element method. Int J Plast 2016;79:48–67.
[15] Jeong C, Heo Y-U, Choi J, Woo W, Choi S-H. A study on the micromechanical behaviors of duplex stainless steel under uniaxial tension using ex-situ experimentation and the crystal plasticity finite element method. Int J Plast 2015;75:22–38, Special Issue: Metal Forming – Challenges in Constitutive and Fracture Modeling.
[16] Bugat S, Besson J, Pineau A. Micromechanical modeling of the behavior of duplex stainless steels. Comput Mater Sci 1999;16(1):158–66.
[17] Aslan O, Cordero N, Gaubert A, Forest S. Micromorphic approach to single crystal plasticity and damage. Internat J Engrg Sci 2011;49:1311–25.

[18] Sabnis P, Forest S, Cormier J. Microdamage modelling of crack initiation and propagation in FCC single crystals under complex loading conditions. Comput Methods Appl Mech Engrg 2016;312:468–91.
[19] Lindroos M, Laukkanen A, Andersson T, Vaara J, Mantyla A, Frondelius T. Micromechanical modeling of short crack nucleation and growth in high cycle fatigue of martensitic microstructures. Comput Mater Sci 2019;170:109185.
[20] Lindroos M, Isakov M, Laukkanen A. Crystal plasticity modeling of transformation plasticity effects, adiabatic heating, and a damage approach for metastable austenitic stainless steels. Int J Mech Sci 2020. submitted.
[21] Cailletaud G, Pilvin P. Utilisation de modèles polycristallins pour le calcul par éléments finis. Revue Européenne Des éléments 1994;3(40):515–41.
[22] Holmberg K, Laukkanen A, Turunen E, Laitinen T. Wear resistance optimisation of composite coatings by computational microstructural modelling. Surf Coat Technol 2014;247:1–13.
[23] Holmberg K, Laukkanen A, Ghabchi A, Rombouts M, Turunen E, Waudby R, Suhonen T, Valtonen K, Sarlin E. Computational modelling based wear resistance analysis of thick composite coatings. Tribol Int 2014;72:13–30.
[24] Laukkanen A, Pinomaa T, Holmberg K, Andersson T. Effective interface model for design and tailoring of WC–Co microstructures. Powder Metall 2016;59(1):20–30.
[25] Lindroos M, Laukkanen A, Andersson T. Micromechanical modeling of polycrystalline high manganese austenitic steel subjected to abrasive contact. Friction 2019;10:1237.
[26] Wallin K, Nevasmaa P, Laukkanen A, Planman T. Master curve analysis of inhomogeneous ferritic steels. Eng Fract Mech 2004;71(16):2329–46.
[27] Lindroos M, Scherer J-M, Forest S, Laukkanen A, Andersson T, Vaara J, Mantyla A, Frondelius T. Micromorphic crystal plasticity approach to damage regularization and size effects in martensitic steels. Int J Plast 2020. submitted.
[28] Kim S, Marrow T. Application of electron backscattered diffraction to cleavage fracture in duplex stainless steel. Scr Mater 1999;40(12):1395–400.
[29] Pilhagen J, Sieurin H, Sandström R. Fracture toughness of a welded super duplex stainless steel. Mater Sci Eng A 2014;606:40–5.
[30] Kolednik O, Albrecht M, Berchthaler M, Germ H, Pippan R, Riemelmoser F, Stampfl J, Wei J. The fracture resistance of a ferritic-austenitic duplex steel. Acta Mater 1996;44(8):3307–19.
[31] Pilhagen J, Sandström R. Influence of nickel on the toughness of lean duplex stainless steel welds. Mater Sci Eng A 2014;602:49–57.
[32] Tonizzo Q, Caillard D, Perlade A, Mazière M, Gourgues-Lorenzon A. Multiscale examination of deformation and fracture mechanisms of a duplex advanced high strength steel: Effect of testing temperature and of micromechanical interactions between microstructural constituents. Mater Sci Eng A 2019;764:138196.
[33] Pinomaa T, Yashchuk I, Lindroos M, Andersson T, Provatas N, Laukkanen A. Process-structure-properties-performance modeling for selective laser melting. Metals 2019;9(11).
[34] Pinomaa T, Lindroos M, Walbrühl M, Provatas N, Laukkanen A. The significance of spatial length scales and solute segregation in strengthening rapid solidification microstructures of 316L stainless steel. Acta Mater 2020;184:1–16.
[35] Qian G, Lei W-S, Niffenegger M, Gonzlez-Albuixech VF. On the temperature independence of statistical model parameters for cleavage fracture in ferritic steels. Phil. Mag. 2018;98:959–1004.
[36] Liu Z, Wang X, Miller RE, Hu J, Chen X. Ductile fracture properties of 16mnd5 bainitic forging steel under different in-plane and out-of-plane constraint conditions: Experiments and predictions. Eng. Fracture Mech. 2021;241:107359.
[37] Qian G, Lei W-S, Peng L, Yu Z, Niffenegger M. Statistical assessment of notch toughness against cleavage fracture of ferritic steels. Fatigue Fract. Eng. Mater. Struct. 2018;41:1120–31.